PROGRESS IN UNDERSTANDING THE PHYSICAL PROCESSES INSIDE SPINNING CONE COLUMNS

T.A.G. Langrish, S.V. Makarytchev, D.F. Fletcher and R.G.H. Prince

Department of Chemical Engineering, University of Sydney, Australia 2006.

ABSTRACT

The dynamics of gas flow through spinning cone columns (SCCs) have been studied through Computational Fluid Dynamics (CFD) simulations, and the liquid flow characteristics on the rotating surfaces have been correlated through dimensional analysis.

The CFD simulations have been carried out in the absence of liquid flow. Flow instabilities are predicted above a critical value of the hydraulic Reynolds number (Re^{hyd}, based on the minimum passage size between the cones) of about 100. High-frequency oscillations of the velocity components and pressure are predicted to occur about their mean values. The flow regime is an unsteady laminar one, not a turbulent one, for small-scale SCCs, as shown by the discrete nature of the pulsation spectrum across the entire range of the column operation ($200 < Re^{hyd} < 2000$) irrespective of whether or not the inner cone is rotating (as in normal operation). The pulsations are synchronised with the rotor motion for normal (rotating) operation and are likely to cause mechanical vibrations as a consequence of the flow instability. The actual pressure drop through the column stage is predicted by the CFD model to within 10-15%.

Key parameters determining mass transfer characteristics and overall performance of SCCs include the thickness and velocity of the thin liquid films flowing up a rotating cone surface. The turbulent flow conditions of commercial-scale equipment make laminar model predictions for these devices inapplicable. Dimensionless empirical models for the average thickness and radial velocity of wavy film have been developed based on thickness measurements on a laboratory-scale cone. These measurements were made using the intensity of induced fluorescence of a flowing film illuminated by an ultraviolet light source. The film is modelled as a wavy layer on top of a laminar sub-layer attached to the disk surface, with the thickness of the film being an additive modification of the Nusselt model thickness $\delta^+ = \delta_N^+ + \delta_{wave}^+ = 0.91\eta^{-2/3} + 1.95\eta^{-3}$, where η is a normalised radial distance. The thickness of the wavy layer δ_{wave}^+ has been correlated with 95% confidence limits of $\pm$12%. The proposed models, in dimensional form, express the film thickness and

radial velocity as functions of cone geometrical and operating parameters. Independent velocity measurements on a rotating cone, and film thickness measurements on rotating disks, support this correlation. The normalised film thickness is predicted to be preserved for spinning cone columns of varying size scaled at constant relative capacity.
This work is part of a program to develop a virtual computer model of SCCs for future design and optimization of this type of equipment.

Keywords: CFD; transient flows; rotating cone; liquid film flow; wavy films; film thickness; empirical model.

INTRODUCTION

A SCC consists of a vertical succession of alternate rotating and stationary cones (Fig. 1). Liquid flows as a film down the stationary cone, drains into the base of the rotating cone, and moves upward on the rotating cone again as a film by the action of the centrifugal force. Gas flows up the column countercurrent to the flow of the liquid. Mass transfer from the liquid to the vapour phase in a SCC takes place through the large surface area of the film (which may be less than 1 mm thick), and through the liquid spray in the regions between spinning and stationary cones. There may be several dozen cone sets (stages) in a commercial column. A feature of the columns as manufactured by Flavourtech, PO Box 413, Griffith Australia 2680, is the fins attached to the lower surfaces of the spinning cones. The fins act as a centrifugal pump to an extent, giving some control of pressure along the column.

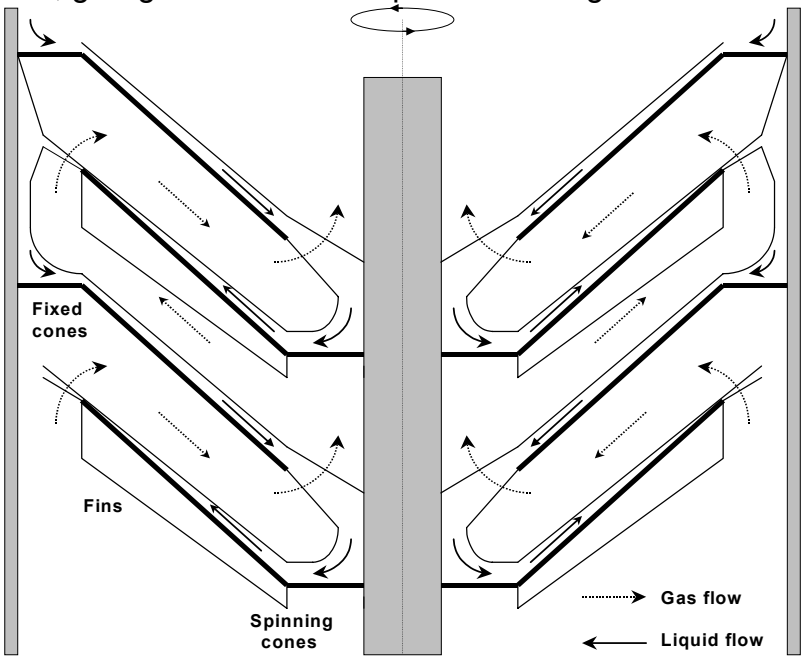

Fig. 1. A section through part of a SCC.

A typical application of SCCs is adding value to quality fruit juices or to instant coffee by extracting flavours before any other processing (pasteurisation, concentration), followed by flavour re-injection at the last feasible time, giving a true-flavour product. Other applications include alcohol modification in wines. These examples exploit the key capabilities of a SCC in handling thermally-sensitive materials and tolerating the presence of solids. SCCs give good pressure control due to the presence of fins and

rotation, which is important in the processing of thermally sensitive materials, since these are frequently separated under vacuum to keep temperatures low, and the temperatures are directly linked to the operating pressures.

In earlier work, we developed a design approach based on empirically established procedures and correlations (Prince *et al.*, 1997). The hydrodynamic regimes and the spatial structure of the liquid film flow over a rotating cone surface have now been studied by us (Makarytchev *et al.*, 1998; Al-Hawaj, 1999). We have developed correlations for the thickness and the average velocity of the wavy liquid film on such surfaces (Makarytchev *et al.*, 2001a). Although there is a considerable amount of work on liquid flow over rotating conical surfaces (Charwat *et al.*, 1972; Matsumoto *et al.*, 1973; Muzhilko *et al.*, 1983; Shvets *et al.*, 1992; as reviewed by Makarytchev *et al.*, 2001a), this work has not yet been integrated with assessments of the gas flow behaviour in processing equipment.

This work reviews progress in understanding the physical processes inside SCCs, specifically the behaviour of liquid films on the spinning cone columns, and the gas-only flow patterns.

LIQUID FILM BEHAVIOUR

The behaviour of thin liquid films spread out on a rotating cone surface significantly influences the mass transfer characteristics and capacity of spinning cone distillation columns (SCC), centrifugal film evaporators and atomisers, and similar gas-liquid contacting devices. The thickness of the film and the shape of its surface are among the key parameters affecting the mass and the momentum transfer from the liquid to the vapour phase. Existing theoretical and experimental evidence suggests that the waviness on the film surface and the turbulence in the adjacent vapour stream enhance the transfer rates (Javdani, 1974; Hirschburg and Florschuetz, 1982; Chen, 1989). Recent experimental studies of SCCs have confirmed that the mass-transfer rates in the commercial-size apparatus are 3-5 times higher than those expected for laminar liquid and vapour flow over the cones (Prince *et al.*, 1997). Since the flow regime in a commercial SCC has been shown to be turbulent (Makarytchev *et al.*, 1998), this enhancement can be attributed to the waviness of the film surface.

For rotating disks, it is known that the average thickness of a wavy film is 40-50% greater than that predicted by laminar theory (Espig and Hoyle, 1965). We could expect therefore that the laminar models available for the liquid film flow over the cone – adaptation of the classic Nusselt model and the modified model of Bruin (Bruin, 1969; Makarytchev *et al.*, 1997) – would also be inapplicable under the turbulent flow conditions of commercial-scale equipment. For immediate engineering applications, an empirical correlation of experimental data would then be useful.

We have more recently (Makarytchev *et al.*, 1998). developed such a correlation based on measurements of the film thickness on a laboratory-scale rotating cone in an unbounded environment. This study is a first approximation to the situation in a SCC, in which a stationary cone is located above each rotating cone. The analysis of the experimental data employs a dimensionless number approach to the problem as

developed by us previously (Makarytchev *et al.*, 1998). The essence of this approach is the characterisation of the liquid flow regime by the combined Reynolds number:

$$Re^{comb} = \frac{Q_0 \omega r \sin\beta}{\nu_G \nu_L}, \qquad (1)$$

and normalisation of the physical coordinates:

$$\eta = \frac{r}{r_0}, \qquad r_0 = \left(\frac{4Q_0^2}{\pi^2 \omega \nu_L \sin^3\beta} \right)^{1/4}, \qquad (2)$$

$$\sigma = \frac{s}{\delta_E}, \qquad \delta_E = \left(\frac{\nu_L}{\omega \sin\beta} \right)^{1/2}.$$

We have shown that in terms of Re^{comb}, η and σ, the regions of different hydrodynamic regimes and the spatial structure of the flow (i.e., division of the overall flow domain into zones with different balances of forces) can be summarised as:
flow regimes: laminar ($Re^{comb} < 1.0 \cdot 10^5$), wavy-laminar ($1.0 \cdot 10^5 < Re^{comb} < 1.0 \cdot 10^6$), and fully turbulent ($Re^{comb} > 1.0 \cdot 10^6$);
flow zones: inner inlet-dependent zone for $\eta<0.8$ (with boundary layer flow for $\sigma<1.5$ and quasi-geostrophic flow for $\sigma>1.5$), intermediate Coriolis zone for $0.8<\eta<2.0$ (boundary layer flow), and outer centrifugal zone for $\eta>2.0$ (boundary layer).

Expressed in the dimensional terms, these results form the basis of a flow diagram that relates flow structure and regimes to the cone geometrical and operating parameters. This approach has been used by us for correlating measured thicknesses of the wavy liquid film in the dimensionless form of $\delta^+=\delta^+(\eta)$ and, based on this correlation, for deriving an empirical model $U_{av}=U_{av}(\eta)$ for the average radial velocity of the film. Converted back to dimensional form, these models express the film thickness and radial velocity in terms of cone operating conditions (liquid flowrate, rotational speed), geometrical parameters (cone angle, distance from the axis), and liquid characteristics (density, viscosity).

Our laboratory scale experimental work has been reported in detail in our 2001 reference.

Film thickness correlation
The film thickness measurements have been normalised using the vertical and the radial scale definitions, eq. (2), and tested against two parameters: the combined Reynolds number Re^{comb} and the dimensionless radial distance $\eta=r/r_0$. Plotting the normalised thickness $\delta^+=\delta/\delta_E$ against η showed an evident trend towards an increase with decreasing η. In contrast, plotting δ^+ against Re^{comb} showed random scatter of data points, which pointed to the independence of the normalised thickness with respect to the Reynolds number. It was deduced therefore that a change of the flow regime, which in our experiments was transitional from wavy-laminar to turbulent, does not affect the average thickness of the film. Physically this means that films with different surface shapes (regular wavy or chaotically rippling) have the same average thicknesses. This finding allows correlation of the measured thickness in the simple form $\delta^+=\delta^+(\eta)$. When the experimental data are compared as a plot of the normalised thickness δ^+ against the dimensionless radial distance η with predictions by two laminar models: the linear Nusselt model and the non-linear numerical solution by

Shvets *et al*. (1992), the increase of measured thickness with decreasing η is faster than that predicted by laminar models. This reflects the presence of waves on the surface of the liquid, which are not accounted for in the laminar models, and which have been confirmed by visual observations. The increase is most notable in the inlet and the Coriolis zones (η<2), where this disturbance of the surface is significant. At large radial distances, the scale of the waviness decreases due to the reduction in film depth, and in the centrifugal zone (η>2) our measurements agree with the laminar models.

Experiments on rotating disks suggest that a gradual transition from turbulent flow to laminar with a perturbed film surface occurs when the thickness of the film becomes comparable with the thickness of the laminar sub-layer attached to the disk surface (Butuzov and Pukhovoi, 1976). There is also experimental evidence that, for all the flow regimes (laminar, wavy-laminar, or turbulent), the Nusselt (laminar) model predicts correctly the thickness of the film in the far centrifugal zone (Charwat *et al.*, 1972; Matsumoto *et al.*, 1973; Lepekhin *et al.*, 1981; Muzhilko *et al.*, 1983). A physically reasonable form of a correlation is an additive correction to the laminar model, which we represent here by the dimensionless Nusselt formula (Makarytchev *et al.*, 1998):

$$\delta^+ = \delta_N^+ + \delta_{wave}^+ = 0.91\eta^{-2/3} + \delta_{wave}^+(\eta)\,. \qquad (3)$$

The correlation in the form of eq. (3) implies physically that the waves roll over the laminar sub-layer and do not penetrate through the latter, but increase the average thickness of the film. A plausible relationship between the dimensionless thickness of the wavy layer and the operating parameters is

$$\delta_{wave}^+(\eta) = \delta^+ - \delta_N^+ = A\eta^B = A\left[\frac{r}{\left(4Q_0^2/\pi^2\omega\nu_L\sin^3\beta\right)^{1/4}}\right]^B, \qquad (4)$$

where *A* and *B* are constants. Over its range of validity, an analysis of variance for the logarithm of the deviation between the measured film thickness and the Nusselt thickness ($\log(\delta^+_{exp}-\delta^+_N)$) against the logarithms of liquid flowrate, rotational speed and radius should then give no significant interaction terms between these variables, as we have shown to be the case (Makarytchev *et al.*, 2001). We have also considered the possibility of alternative forms for the correlation between the measured film thickness and the operating parameters, including a simple power-law relation, $\delta^+ = A\eta^B$, and a multiplicative correction to the Nusselt model, $\delta^+ = A\eta^B\delta_N^+$. The analyses of variance for these alternative forms also show insignificant interaction terms. However, these forms of correlation, albeit statistically comparable with the additive form, we rejected as having not as clear a physical basis.

Model parameters *A* and *B*, eq. (4), were determined by linear regression of the logarithm of $\delta^+_{exp}-\delta^+_N$ with respect to the logarithm of η. The limits of 95% confidence in the correlation correspond to a relative range of ±12% on the original arithmetical scale. After rounding the slope coefficient to an integral value within the confidence limits, the full dimensionless form of the correlation became :

$$\delta^+ = 0.91\eta^{-2/3} + 1.95\eta^{-3}\,. \qquad (5)$$

This correlation and its confidence limits are shown in Fig. 2. At small η, the wavy layer is dominant in determining the average film thickness. As η increases, δ^+_{wave} approaches zero faster than δ^+_N, representing a decrease in the surface waviness in the region further from the axis. In the far centrifugal zone (η>>1) the correlation converges to the Nusselt model.

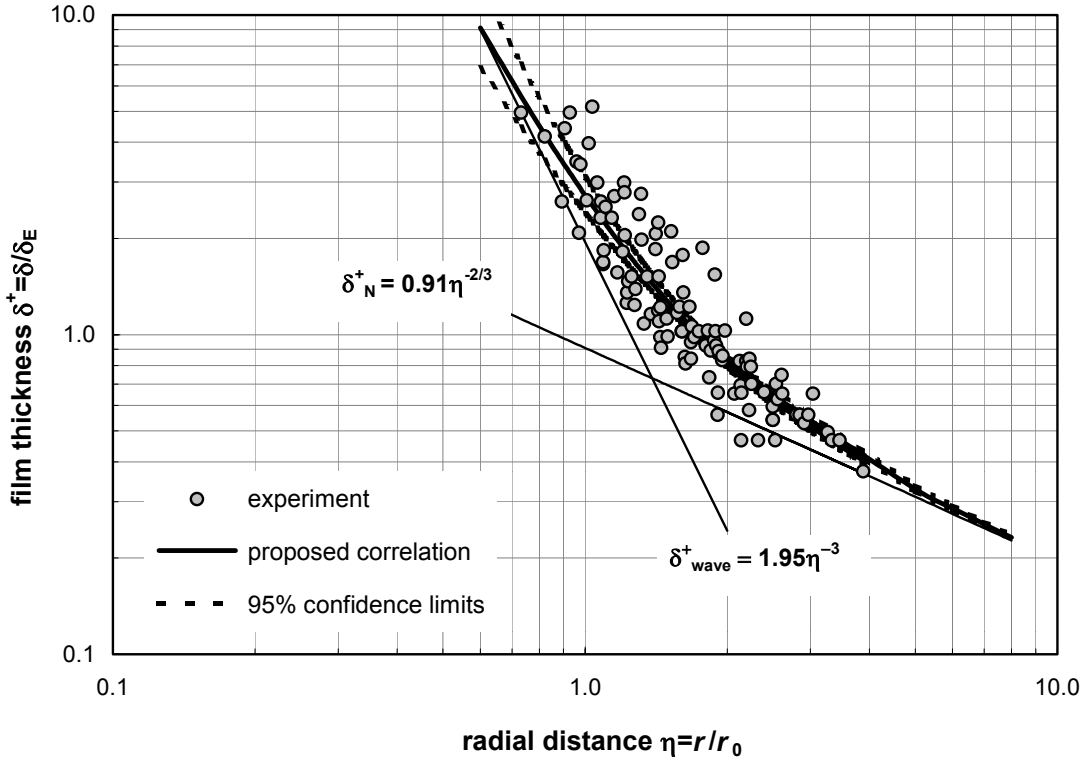

Fig. 2. Correlation for the film thickness

When converted to dimensional form, the correlation expresses the film thickness in terms of the geometrical parameters (radial distance along the cone surface, cone apex angle), operating parameters of the column (liquid flowrate, rotational speed), and characteristics of the liquid (density, dynamic viscosity):

$$\delta = \delta_N + \delta_{wave} = 0.78\frac{Q_0^{1/3}\nu^{1/3}}{\omega^{2/3}r^{2/3}\sin\beta} + 0.48\frac{Q_0^{3/2}}{\omega^{5/4}\nu^{1/4}r^3\sin^3\beta}. \qquad (6)$$

Average radial velocity

The film thickness correlation leads to an empirical model for the average radial velocity, which can be expressed again as a correction to the Nusselt model:

$$U_{av} = \frac{0.28\eta^{-4/3}}{1+2\eta^{-7/3}} \equiv \frac{U_{av,N}}{1+2\eta^{-7/3}}. \qquad (7)$$

Some early velocity measurements reported in our 2001 reference give direct support to this correlation, which meets the physically evident condition that the radial velocity component should disappear at the axis of rotation where the only component of the velocity is vertical. The non-linear Shvets model shows a similar initial trend but with

a rapid decrease in the velocity at the model limit of η=0.8. Both convergence to the Nusselt model prediction at large radii.

Applicability of the results to larger scale equipment

Figure 4 shows the location of the domain of experimental conditions on a diagram of the flow zones and regimes developed earlier (Makarytchev *et al*., 1998). In this diagram, the lower pair of horizontal lines represents the radial extent of the rotating cone surface for our apparatus (0.06-0.2 m) at the limiting flowrates of 1.4 and 6.0 L/min. The upper pair of lines corresponds to a standard commercial SCC operating in a liquid flowrate range of 33-170 L/min. The inclined solid lines in the lower-left to upper-right direction of the diagram are the boundary between the inlet zone and the inlet-independent Coriolis zone (η=0.8) for rotational speeds of 250, 500, and 1000 rpm. The parallel triplet of dashed lines is the boundary of the centrifugal zone (η=2), below which the Nusselt model applies. The other set of lines (in the up-left to down-right direction) separates the regions of different flow regimes: laminar below the dashed lines (Re^{comb}<1.0·10^5), turbulent above the solid lines (Re^{comb} >1.0·10^6), and wavy-laminar in between.

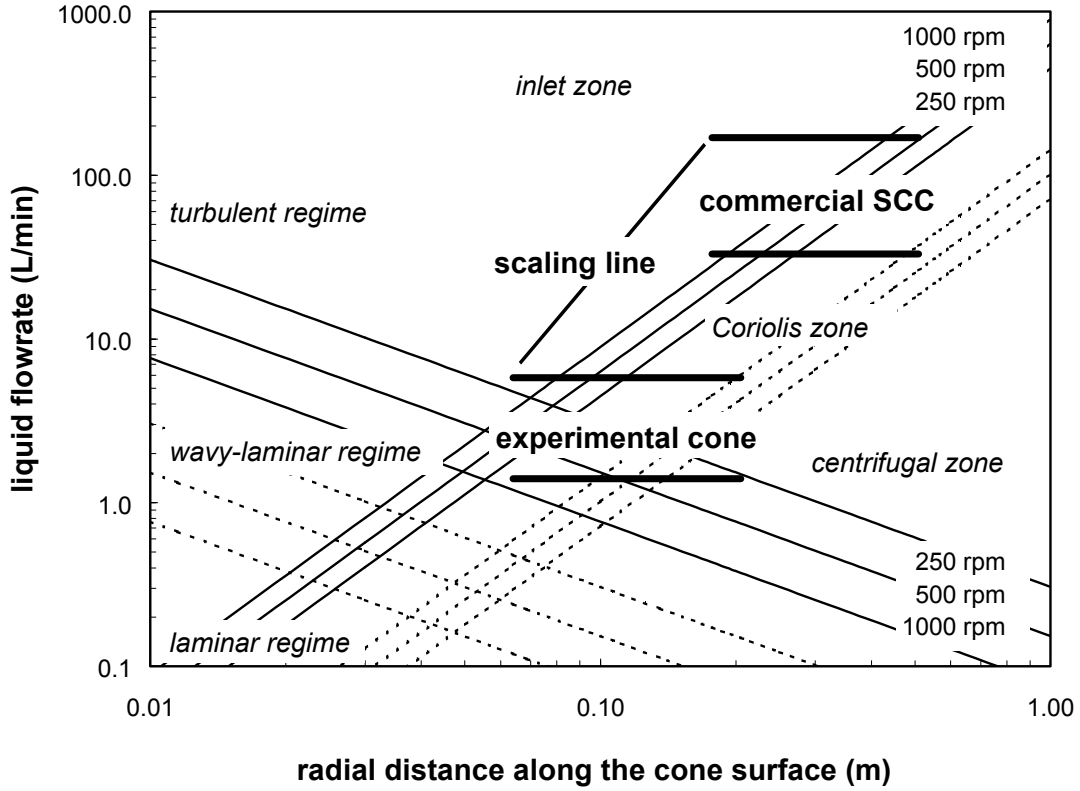

Fig. 4. Operating conditions of experimental cone and commercial SCC, and the boundaries of the flow zones and regimes.

The "scaling" line in Fig. 4 shows explicitly a line of constant relative capacity (constant proportion of flooding onset). This direction is almost parallel to the lines of constant η – the lines of liquid flow similarity (slopes 2.5 and 2.0, respectively). The similar positions of the experimental and the commercial operation domains relative to the lines of constant η indicate similarity of the flow structure, in terms of similar spatial location of the flow zones.

Correlations of data obtained on experimental equipment may be related to commercial scale by the dimensionless parameters η and Re^{comb}, where the former allows for change of the flow structure and the latter for difference in the flow regime. Figure 4 implies that the structure is essentially preserved on scaling (η remains almost constant along a "scaling line") while the regime changes significantly from laminar-wavy for laboratory scale to fully turbulent for commercial scales.

For average film thickness, the parameter Re^{comb} was shown to be not significant. Both the film thickness and the average radial velocity depend on the dimensionless radial distance η only, as defined by eqs. (5) and (7), respectively. Therefore, δ^+ and U_{av} also remain almost constant along a "scaling line", i.e., on appropriate scale-up.

GAS-ONLY FLOW PATTERNS

The gas flow regime and the associated pressure drop through the column have the practical significance of being an approximation to the actual situation in a SCC for small liquid loads. To address the complex internal geometry of the column, we have used a Computational Fluid Dynamic (CFD) approach to analyse the fluid flows. Use of CFD analysis is particularly necessary due to the presence of fins, the number and design of which affect the topology of the CFD model and the computational approach used (rotating coordinates). The base-case CFD model for gas-only flow in SCCs is a basis for analysing the more complex gas-liquid (two-phase) flows, as a starting point for future optimisation of SCC design and operation.

Previous measurements, CFD modelling and CFD analysis of flow patterns has been carried out for conventional distillation column trays (Porter *et al.*, 1992; Yu *et al.*, 1999; Liu *et al.*, 2000). Wagenaar *et al.* (1994) modelled and measured particle dynamics and gas-phase flow in a rotating cone reactor, with the gas flow being treated with a boundary layer approximation. They commented that "*A more accurate description of the flow behaviour of the gas phase can be obtained if a computational fluid dynamics (CFD) model is applied.*" Such a CFD analysis has been carried out for a spinning cone column, which involves strongly swirling, transitional flows.

A laboratory-scale SCC, for which detailed experimental data (pressure drop, flooding characteristics, mass-transfer coefficients) are available, has been described by us earlier (Prince et al. 1997, Sykes 1996) and has been used as the basis for the CFD geometry.

The CFD model – numerical considerations

The simulations used the Computational Fluid Dynamics (CFD) program CFX4.3™, which uses a structured mesh and a finite volume formulation to discretise the Navier-Stokes equations. These equations describe the fluid flows in this equipment and comprise equations for conservation of mass and momentum in this isothermal situation. Full details of the equations and the numerical scheme are given in the User Manual (CFX, 1997). A discussion of various convection schemes is given in Shore et al. (1996). This study showed that the high order schemes implemented in CFX4.3 could reproduce the swirl flow velocity fields obtained using orthogonal grids aligned with the flow using non-orthogonal, non flow aligned grids. The Van Leer

limiter (see Hirsch, 1990) was implemented for all the velocity components. This scheme is second order accurate and maintains monotonicity across computational cells, hence preventing numerical oscillations in the solution domain. The SIMPLEC algorithm (Patankar, 1980) was used for pressure correction. The working fluid, gas, was taken as incompressible and Newtonian. As a convergence criterion, the sum of the absolute mass source residuals over all cells was less than 0.1% of the total flowrate. This resulted in a sufficient number of iterations being carried out for each time step so that changes in monitoring point values were not discernible with further iterations. The variation of residual values with iterations were checked to ensure that the residuals for all the equations were consistently decreasing and approaching their limit of the accuracy for single precision. This minimised the chance of error accumulation over successive time steps. No turbulence model was used here, and the unsteady nature of the flow was resolved by transient simulations.

The solution

With 30×40×40 cells per stage grid, the solution speed on a DEC Personal Workstation 500 *was* about 400 iterations per hour. It then took less than an hour for a well-converged steady state solution (at low Reynolds numbers), and up to several days for a sufficiently long transient run (~0.1 physical second per day of computation). The predicted pressure drop was found to be mesh-independent within 10% compared with the use of a grid as coarse as 18×24×24 cells per column stage. The time step used was 0.1 ms for most of the simulations, for which typically 10 iterations per time step were required to reduce the residual to the required value. This time step is much smaller than that required to resolve the frequency spectra.

Flow regime: Reynolds numbers

The hydrodynamic regime of the flow is characterised by the Reynolds numbers. Those related to this flow situation are: (i) a "hydraulic" Reynolds number, Re^{hyd}, for a flow in a duct, based on a hydraulic radius R_H (in SCC, the minimum width of passage between the cones, Fig. *1*):

$$Re^{hyd} = \frac{VR_H}{\nu} = \frac{Q}{2\pi R_{FI}\nu}, \qquad (8)$$

(ii) a "rotational" Reynolds number, Re^{rot}, for an unbounded fluid flow over a rotating disk:

$$Re^{rot} = \frac{\omega R^2}{\nu} = \frac{\omega R_{SO}^2}{\nu}. \qquad (9)$$

These estimates *give* upper values – the Reynolds number is less elsewhere in the SCC, since the radius in equation (10) is the smallest physical value, and that in equation (11) is the largest physical value.

For the ideal cases of a straight pipe and an unbounded rotating disk, the onset of the first instability and of fully developed turbulence is characterised by the following critical values of these numbers (Moody and Princeton, 1944; Kobayashi, 1994):

Flow regime:	unstable	fully turbulent	
Re^{hyd}	> 2000	> 3000	(pipe)
Re^{rot}	> 0.9×10^5	> 3.2×10^5	(disk)

Table 1 shows the range of the column operating conditions and the corresponding ranges of the Reynolds numbers in this case.

Table 1. The operating conditions for this SCC.

Parameter	Value
Flowrate of gas, Q (l/min)	40-400
Hydraulic Reynolds number, Re^{hyd}	202-2020
Rotational speed, ω (rpm)	500-1500
Rotational Reynolds number, Re^{rot}	$(0.14\text{-}0.43)\times10^5$

Since the ranges of both Reynolds numbers are below the critical values for pipes and disks respectively, the gas flow may be expected to be laminar. In respect to Re^{hyd}, the flow would become increasingly prone to instability when the gas flowrate approaches its critical value of ~ 400 l/min. In relation to rotation, the flow may be expected to be stable up to a rotational speed of about 3000 rpm, which is beyond the normal range of operation. However, the above stability criteria are for ideal cases of straight pipe and unbounded rotating geometries. The actual stability of the flow in equipment as complex as SCCs must be investigated. This necessitates the use of transient calculations.

Steady sub-critical flow

The simulations show*ed* that the steady-state flow regime in this SCC exists only at very low gas flowrates. In the absence of rotation, the critical Reynolds number for the onset of the first instability has been found to be as low as Re^{hyd}_{crit} = 100 (Q = 20 l/min). The steady state flow pattern at $Re^{hyd} < Re^{hyd}_{crit}$ is characterised by the absence of recirculation zones and complete axial symmetry. The maximum values of the velocity and pressure gradients coincide with the minimum flow area between the rotating and the stationary cones. This steady state regime, however, is of little practical relevance since it only occurs below the range of typical SCC operating conditions.

Unsteady flow

At values of Re^{hyd} above the critical value of 100, the flow becomes unstable. Flow pulsations develop after a period of about one residence time ($\tau_{res} = Q / V_{column}$). The spectrum of established velocity pulsation at $\tau > \tau_{res}$ is shown in Fig. 5, as tangential velocities. The spectra for this and other velocity components are discrete. The multiplicity of the modes of pulsation reflects the geometric complexity of the model, since there are many length scales within the column stage. The discrete nature of the spectra suggests that this behaviour reflects flow instabilit*ies* and not fully-developed turbulence, because turbulence would be characterised by continuous power spectrum across a range of frequencies. It is worth mentioning that, at present, there are no developed true models for transitional flows: the low Reynolds number turbulence models available are actually high Reynolds number models that allow integration of the turbulence equations to the wall.

The unsteady flow pattern differs from the steady one. It is characterised by the presence of multiple eddies (recirculation zones) in the corners of the inner and outer throat and even between the cones at higher flowrates (Fig. 6).

The maximum values of velocity are now located underneath the rotating cone. The pressure drop is largest in the inner throat region of the column where the changes of velocity direction and magnitude are most significant.

To investigate these pulsations in more detail, several snapshots of the flow field at time intervals of 0.1 s have been plotted. Investigation of the results has shown that while the macroscopic structure of the flow field is basically preserved, the pulsations correspond to small chaotic displacements of the flow streamlines, formation and disappearance of additional eddies, and other irregularities of the flow pattern. The most significant disturbances occur in the inner and the outer throat regions, where the flow changes its direction. These frequent changes of the flow direction and area are reasons for the inherent flow instability and the lower value of the critical Reynolds number for gas flow in SCCs (~100) compared with that for pipe flows (~2000).

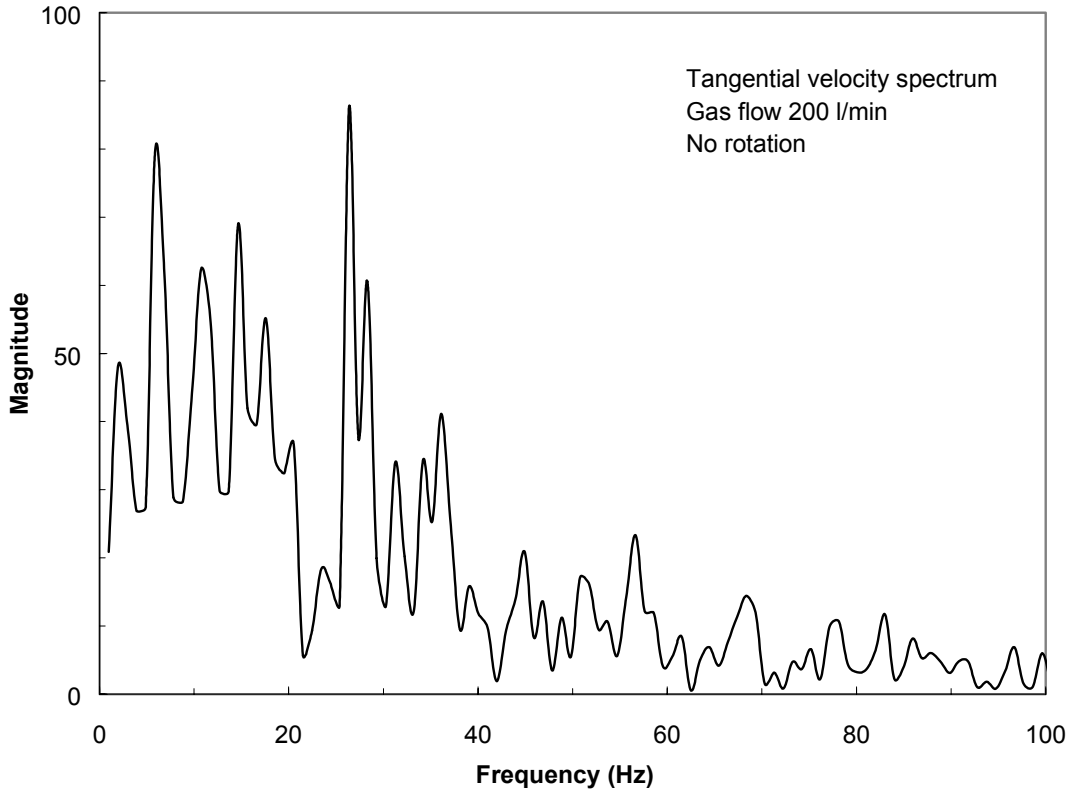

Fig. 5. Spectrum of velocity pulsations with no rotation, gas flowrate 200 l min^{-1}.

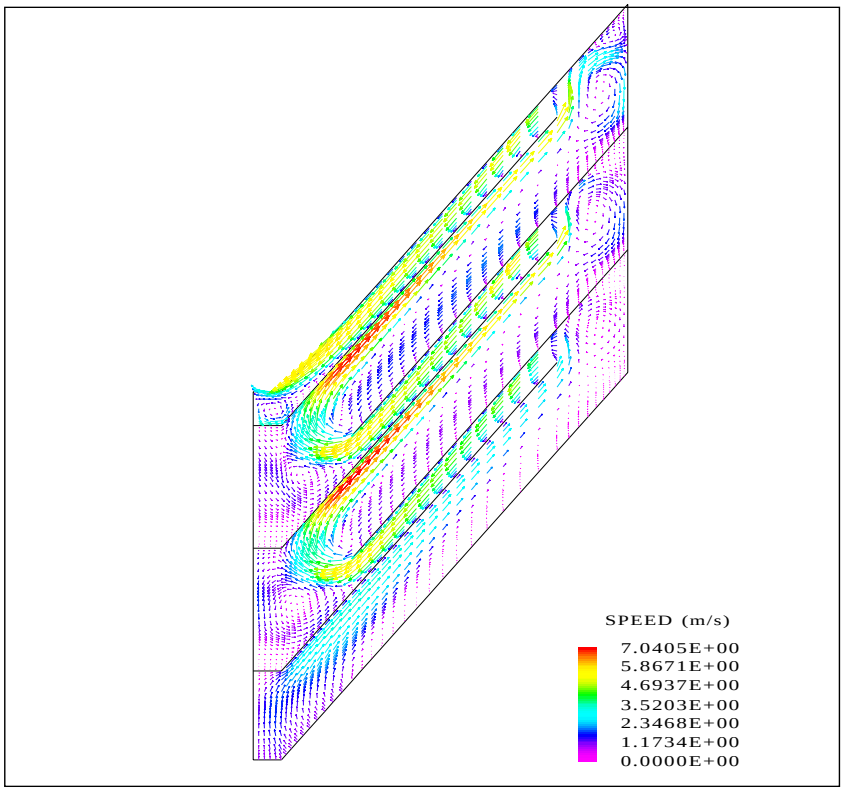

Fig. 6. A snapshot of the flow pattern for no rotation, gas flowrate 200 l min^{-1}.

Effect of rotation

Adding rotation affects both the character of the pulsations and the flow pattern. Instabilities now develop faster than in the no-rotation case, at $\tau > \tau_{rot} = (\omega)^{-1}$. These instabilities are forced oscillations in an already unstable flow system driven by the rotor motion. The spectrum of pulsation becomes simpler than that for the case of no rotation, since the presence of regular motion removes some of the spectral lines and decreases the magnitude of others. The frequency of fins passing a fixed spatial point ($3\times\omega$) is always present in the spectrum. At higher rotational speeds this frequency becomes the dominant mode of oscillation. Changing the rotor speed leads to a corresponding shift of this dominant mode. Thus there is a clear effect of synchronisation of the flow pulsation by the rotor motion. The rotation results in a significant increase of both the velocity and the pressure in the outer throat region. These aspects make the distribution of flow parameters more homogeneous in the radial direction. In the tangential direction, the flow pattern becomes asymmetric. The regions of maximum velocity and pressure gradient are now located in the vicinity of fins. These results and phenomena are described in more detail in Makarytchev et al. 2002

Pressure drop: Comparison with experiment

Due to velocity oscillations, the pressure also pulsates, so that time averaging is required for comparison of the pressure drop with experiment. The pressure drop has been calculated as the difference between entry and exit pressure values averaged over a 0.1-0.3 s time interval after a transitional period corresponding to the residence time of gas in the system ($\tau > \tau_{res}$). The CFD-predicted pressure drops are compared with the measurements in Fig. 7, and the pressure drop is predicted by the CFD model within 10-15% across the entire range of operating conditions. Given the

pulsating nature of the flow and the scatter in the experimental values themselves of around 10%, the agreement of the model predictions with measurements is good.

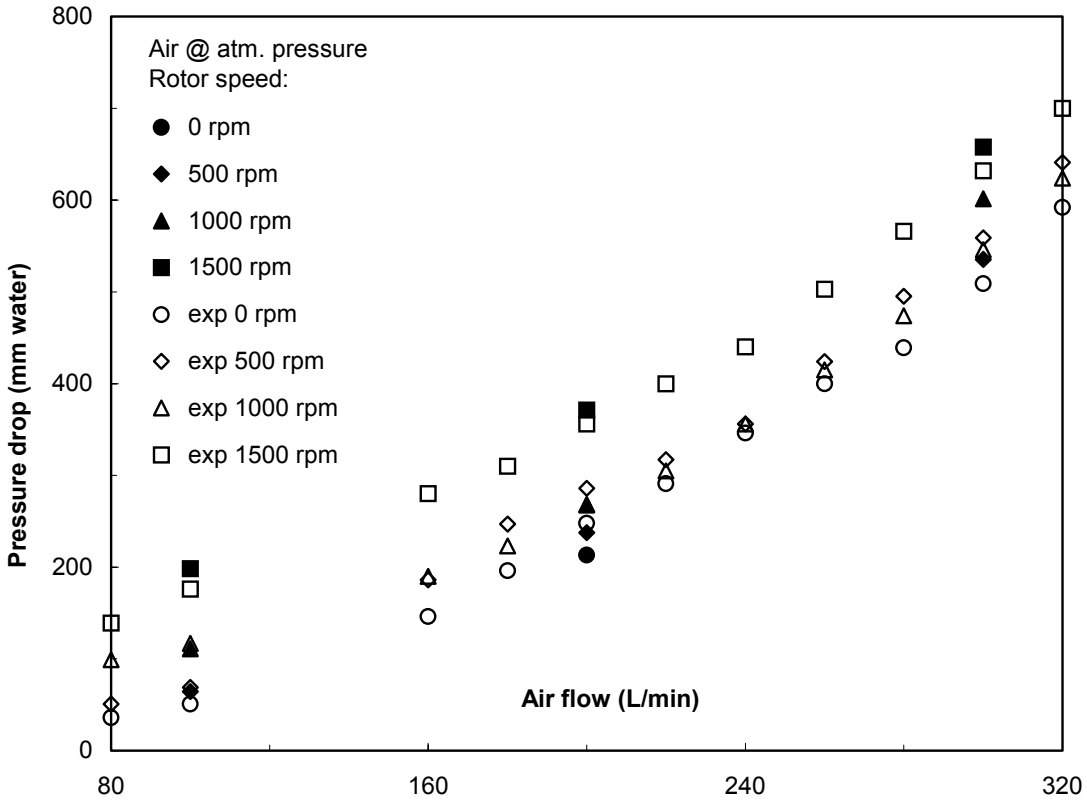

Fig. 7. Comparison of the predicted (black markers) and the measured pressure drops.

Practical implications of pulsations

Under certain operating conditions, pressure pulsations may lead to mechanical vibrations of the column. Due to the effect of synchronisation between the rotor motion and the gas flow pulsation, conditions exist for effective energy exchange between the mechanical and the hydrodynamic parts of an overall SCC system. Significant oscillation power is contained in a low-frequency part of the pressure spectrum even for a three-stage SCC considered in this work. Lower frequencies are possible in a multi-stage (say, forty-stage) SCC. These low frequencies, or their harmonics, may resonate with the mechanical modes of oscillation and excite, for instance, waves propagating up and down along the axis of the column. Thus the mechanical and overall stability of the column operation becomes of practical concern.

CONCLUSIONS

Physical arguments presented here and in earlier work show that the liquid film on a rotating cone surface may be modelled as a wavy layer on top of a laminar sub-layer represented by the Nusselt model. Our experimental data show the total thickness is independent of the Reynolds number, and may then be represented as an additive

modification of the Nusselt model thickness, δ_N^+, in the dimensionless form $\delta^+ = \delta_N^+ + \delta_{wave}^+ = 0.91\eta^{-2/3} + 1.95\eta^{-3}$, where η is a normalised radial distance, and δ_{wave}^+ is here correlated with confidence limits of $\pm$12%. In dimensional form, the proposed models can then express the film thickness and velocity in terms of cone operating conditions (liquid flowrate, rotational speed), geometrical parameters (cone angle, distance from the axis), and liquid characteristics (density, viscosity). The predictive capability of the models is supported by independent velocity measurements on a rotating cone and the film thickness measurements on rotating disks. A useful deduction for design and analysis of operation of spinning cone distillation columns is that the dimensionless film thickness is essentially preserved on scaling at constant relative capacity, but that the liquid flow changes from laminar to turbulent on scaling up.

The gas flow in a SCC under conditions of practical interest (Re^{hyd} >100) is unstable. The instability is manifested as pulsations of the velocity components and pressure around their average values. Spectral analysis of these pulsations indicates that the regime of the flow is an unsteady laminar one, not fully-developed turbulent. This regime occurs across the entire range of operation for the SCC considered ($200<Re^{hyd}<2000$). Time-averaged values of the CFD-predicted pressure drops agree with experiment within 10-15% over the whole range of column operating conditions. Pressure pulsations have been found, which may lead to mechanical vibrations in the equipment and instability of column operation at small liquid loads.

Hydrodynamic causes of vibration (flow pulsation) may be significantly reduced or even entirely eliminated by changes in gas passage design and/or operating parameters of the column. Exploration of the design and operation alternatives requires a model that reflects the detailed geometry of the equipment of interest. The CFD approach to SCC analysis and the computational model of the column being developed in this work are capable of such development and optimisation tasks. However, development of the approach to include two-phase flow is necessary before such tasks can be carried out for this system, and such a development will be carried out in future work.

ACKNOWLEDGEMENTS

The work has been supported by Australian Research Council Large Grants.

NOTATION

A	fitting constant in equation (4)
A_{inlet}	inlet area, m^2
B	fitting constant in equation (4)
P	pressure, Pa
Q	volumetric flow rate of gas, $m^3\ s^{-1}$ or $l\ min^{-1}$
Q_0	volumetric flow rate of the liquid, $m^3\ s^{-1}$ or $l\ min^{-1}$
r	radial distance along the cone surface, m
r_0	characteristic radial distance defined by Eq. (2), m

R_H width of the passage between cones in SCC, m
R_{FI} inner radius of the fixed cone, m
R_{SO} outer radius of the spinning cone, m
Re^{comb} combined Reynolds number defined by Eq. (1)
Re^{hyd} hydraulic Reynolds number defined by Eq. (10)
Re^{rot} rotational Reynolds number defined by Eq. (11)
s distance in the direction perpendicular to the cone surface, m
u_{av} average radial velocity of the liquid film, m s^{-1}
U_{av} dimensionless average radial velocity of liquid (= u_{av}/w_{cone})
$U_{av,N}$ Nusselt model prediction for the average radial velocity of liquid
U_{inlet} inlet gas velocity, m s^{-1}
V characteristic gas velocity, m s^{-1}
V_{column} volume of the column, m^3
w_{cone} tangential velocity of the cone surface (=$\omega r \sin\beta$), m s^{-1}

Greek letters

β half the angle at the apex of the cone, deg
δ dimensionless cross-film coordinate (= s/δ_E), liquid film thickness, m
δ_E thickness of the Ekman layer defined by eq. (1.1), m
δ_N Nusselt model prediction for the liquid film thickness, m
δ_{wave} thickness of the wavy layer, m
δ^+ dimensionless film thickness (= δ/δ_E)
η dimensionless radial coordinate (= r/r_0)
ν_L kinematic viscosity of the liquid, m^2 s^{-1}
ν_G kinematic viscosity of the gas, m^2 s^{-1}
τ_{res} residence time of the gas in the column, s
τ_{rot} characteristic time of rotation, s
Ω angular velocity of the system of coordinates, s^{-1} or rpm
ω angular velocity of the cone rotation, s^{-1} or rpm

REFERENCES

Al-Hawaj, O. (1999) A numerical study of the hydrodynamics of a falling liquid film on the internal surface of a downward tapered cone. *Chem. Eng. J.*, **75**(3), 177-182.

Bruin, S. (1969) Velocity distributions in a liquid film flowing over a rotating conical surface. *Chem. Eng. Sci.* **24**, 1647-1653.

Butuzov, A. I. and Pukhovoi, I. I. (1976) Liquid-film flow regimes on a rotating surface. *J. Eng. Phys.* **31**, 886-891.

CFX 4 (1997) Solver Manual, CFX International, AEA Technology, Harwell, Didcot, Oxon, UK.

Charwat, A. F., Kelly, R. E. and Gazley, C. (1972) The flow and stability of thin liquid films on a rotating disk. *J. Fluid Mech.* **53**, 227-255.

Chen, S. L. (1989) The effect of interfacial waviness on film condensation. *J. Chin. IChE* **20**, 91-99.

Espig, H. and Hoyle, R. (1965) Waves in a thin liquid layer on a rotating disk. *J. Fluid Mech.* **22**, 671-677.

Hirsch, C. (1990) Numerical Computation of Internal and External Flows. Vol. 2, Wiley, New York, 536-545.

Hirschburg, R. I. and Florschuetz, L. W. (1982) Laminar wavy film. *J. Heat Transfer* **104**, 452-458.

Javdani, K. (1974) Mass transfer in wavy liquid films. *Chem. Eng. Sci.* **29**, 61-69.

Kobayashi (1994) Review: laminar-to-turbulent transition of three-dimensional boundary layers on rotating bodies. *Trans. ASME*, **116**, 200-211.

Lepekhin, G. I., Ryabchuk, G. V., Tyabin, N. V. and Shul'man, E. R. (1981) Flow of a viscous liquid over the surface of a rotating flat disk. *Theor. Found. Chem. Engng* **15**, 243-248.

Liu, C.J., Yuan, X.G., Yu, K.T. and Zhu, X.J. (2000) Fluid-dynamic model for flow pattern on a distillation tray. *Chem. Eng. Sci.* **55**(12), 2287-2294.

Makarytchev, S. V., Xue, E., Langrish, T. A. G. and Prince, R. G. H. (1997) On modelling fluid flow over a rotating conical surface. *Chem. Eng. Sci.* **52**, 1055-1057.

Makarytchev, S. V., Langrish, T. A. G. and Prince, R. G. H. (1998) Structure and regimes of liquid film flow in spinning cone columns. *Chem. Eng. Sci.* **53**, 1541-1550.

Makarytchev, S.V., Langrish, T.A.G. and Prince, R.G.H. (2001) Thickness and velocity of wavy liquid films on rotating conical surfaces. *Chem. Eng. Sci.*, **56**(1), 77-87.

Makarytchev, S.V., Langrish, T.A.G. and Fletcher, D.F. (2002) CFD analysis of spinning cone column operation: prediction of unsteady pressure drop and pressure drop in a dry column. Accepted for publication in *Chem. Eng. Journal*.

Matsumoto, S., Saito, K. and Takashima, Y. (1973) The thickness of a viscous liquid film on a rotating disk. *J. Chem. Eng. Jpn.* **6**, 503-507.

Moody, L.F. and Princeton, N.J. (1944) Friction factors for pipe flow. *Trans. Am. Soc. Mech. Eng.* **66**, 671-684.

Muzhilko, A. A., Rifert, V. G. and Barabash, P. A. (1983) Flow of liquid film over the surface of a rotating disk. *Heat Transfer-Soviet Research* **15**, 1-6.

Patankar, S.V. (1980) Numerical Heat Transfer and Fluid Flow. Hemisphere, New York.

Porter, K.E., Yu, K.T., Chambers, S. and Zhang, M.Q. (1992) Flow patterns and temperature profiles on a 2.44 m diameter sieve tray. *Trans. IChemE* **70**(5) 489-500.

Prince, R. G. H., Desho, S. Y. and Langrish, T. A. G. (1997) Spinning cone column capacity and mass-transfer performance. *IChemE Symp. Ser.* **142**, 769-781.

Shore, N. A, Haynes, B. S., Fletcher, D. F., and Sola, A. A. (1995) Numerical aspects of swirl flow computations. *Proceedings of the Seventh Biennial Conference on Computational Techniques and Applications: CTAC95*, May, R. L.; and Easton, A. K., Eds., Melbourne 1995 July 3-5, pp. 693-700.

Shvets, A. F., Portnov, L. P., Filippov, G. G. and Gorbunov, A. I. (1992) Flow of axially symmetric viscous liquid film over surface of rotating disk. *Theor. Found. Chem. Engng* **26**, 749-752.

Sykes, S. J. (1996) Operating characteristics of spinning cone columns. *Ph.D. Thesis*, The University of Sydney.

Thomas, S., Faghri, A. and Hankey, W. (1991) Experimental analysis and flow visualization of a thin liquid film on a stationary and rotating disk. *J. Fluids Engng* **113**, 73-80.

Wagenaar, B.M., Kuipers, J.A.M. and van Swaaij, W.P.M. (1994) Particle dynamics and gas-phase hydrodynamics in a rotating cone reactor. *Chem. Eng. Sci.* **49**(7), 927-936.

Yu, K.T., Yuan, X.G., You, X.Y. and Liu, C.J. (1999) Computational fluid-dynamics and experimental verification of two-phase two-dimensional flow on a sieve column tray. *Trans. IChemE* **77**(6) 554-560.